Season and Interannual Variability in Particulate Matter Size and Composition

4. Single Particle Characterization in Riverside, CA during the SOAR 2005 Campaign: Seasonal Comparisons

i. Introduction

The city of Riverside, California covers ~200 km^2 of area in the eastern Los Angeles (LA) basin and encounters some of the worst air pollution problems in the United States. In 2000, Riverside-San Bernardino was one of the six US metropolitan areas out of 296 that exceeded National Ambient Air Quality Standard levels due to high concentrations of O_3, SO_2 and particulate matter; furthermore, out of the nation's 94 largest metropolitan areas, Riverside-San Bernardino was one of three areas with unhealthy air quality levels for sensitive groups on more than 120 days each year between 1999 and 2002 (139). Great attention and effective policies are needed to alleviate the air pollution problem.

In addition to affecting climate and reducing visibility (140-142), ambient particles with aerodynamic diameters (D_a) less than or equal to 2.5 μm ($PM_{2.5}$) can cause serious adverse health effects (110,143). For example, a strong association was found between $PM_{2.5}$ concentration and mortality rate, particularly cardiopulmonary mortality (110); further, exposure to $PM_{2.5}$ and elemental carbon (EC) can lead to significant deficits in children's lung function growth and increase incidents of asthma (144). The distribution and deposition of inhaled particles strongly depend on particle size with smaller particles penetrating further into the respiratory system and even entering the blood stream (145-147). Therefore, in addition to aiding in source apportionment of aerosols in the LA basin and areas with similar emissions inventories and geographical and meteorological conditions, size-resolved ambient aerosol composition and chemical association will also provide valuable information for health effects studies.

Riverside is located along a typical air parcel pathway crossing the LA basin and is the receptor area of LA air pollutants, which transport east and transform along the way. In previous studies, the major components of $PM_{2.5}$ in Riverside were found to be nitrate, ammonium, EC and organic carbon (OC) by mass (148). Vehicle exhaust is the primary source of carbonaceous particles (EC and OC) (149), and the high ammonium concentrations are mostly influenced by emissions from nearby upwind Chino dairy farms, which is the largest single source of ammonia in the greater LA area (150). In summer, $PM_{2.5}$ concentrations reach maxima during the day due to elevated photochemical reactions as well as increased aerosol transport from the LA area in the west; whereas wintertime $PM_{2.5}$ concentrations peak at night due to the decrease in the altitude of inversion layers (44,45,151). Thus, the aerosol chemical composition and formation mechanisms vary considerably by season.

Numerous studies have been conducted in Riverside and other cities in the LA basin during the last three decades to study urban photochemical smog formation, aerosol transport and evolution across the basin, and size-resolved chemical composition of ambient particles (44,45,148,149,151-155). Recent developments in on-line techniques

for aerosol analysis have enabled high temporal resolution for particle number and size measurements. Studies investigating seasonal variability of particle number concentrations, size distributions, and chemical composition were also conducted in Riverside recently (151,155); however no detailed seasonal comparison is available on temporal variations of individual chemical classes and aerosol mixing state.

Aerosol time-of-flight mass spectrometry (ATOFMS) is an on-line mass spectrometry technique which allows the measurement of size and chemical composition of individual particles in real-time (156). ATOFMS can examine complicated aerosol mixtures on a single particle level and provide quantitative high temporal resolution chemical composition, size distribution, and chemical association information (157), which is useful for source apportionment. Previous continuous ambient ATOFMS measurements in Riverside were conducted in 1996 and 1997 (153,154,158); however, single polarity spectra without wide dynamic range (WDR) were collected, and seasonal differences were not the focus (157). Recent ATOFMS developments have allowed for simultaneous dual polarity collection with WDR, improving our ability to classify particles and identify aerosol associations especially with secondary signatures of nitrate and sulfate.

This paper presents summer and fall seasonal differences in aerosol size distribution, composition, and chemical association in Riverside from continuous ATOFMS single particle measurements. Particles with sizes between 0.2 and 2.5 μm are discussed, along with the meteorological conditions which play an important role in aerosol composition and formation mechanisms. Significant differences are observed between summer and fall temporal variations and percentages of individual chemical species. This work is the first attempt to study the seasonal variability of ambient aerosols using ATOFMS single particle measurements, illustrating the changes in the relative concentrations of the major particle types both by time and by size.

ii. Experimental

a. SOAR Campaign

The Study of Organic Aerosols in Riverside (SOAR) field campaign was conducted in the summer and fall of 2005 on the campus of the University of California, Riverside (UCR) for ambient aerosol characterization and source apportionment (159). The sampling site was located in the southeast of the UCR campus (33°58′18″N, 117°19′22″W), and a map is included in **Figure 25**. Immediately to the east and west of the sampling site are the satellite chiller plant and greenhouses, respectively, and a parking lot with a capacity of 129 parking spaces lies directly to the south. A major freeway (I-60/215) with heavy traffic neighbors the campus to the west and southwest and is ~600 meters away from the sampling site. Due to freeway construction, heavy traffic was observed as early as 3:00 and as late as 22:00. All data are presented in Pacific Standard Time (PST).

b. Ambient Sampling

A standard ATOFMS was housed inside a mobile laboratory from July 30 to August 15 (SOAR-I) and from October 31 to November 21 (SOAR-II) with ~1 hour of downtime daily for maintenance mostly between 20:00 and 21:00. A co-located aerodynamic particle sizer (APS, TSI 3321) and UV photometric O_3 analyzer (TEI 49C)

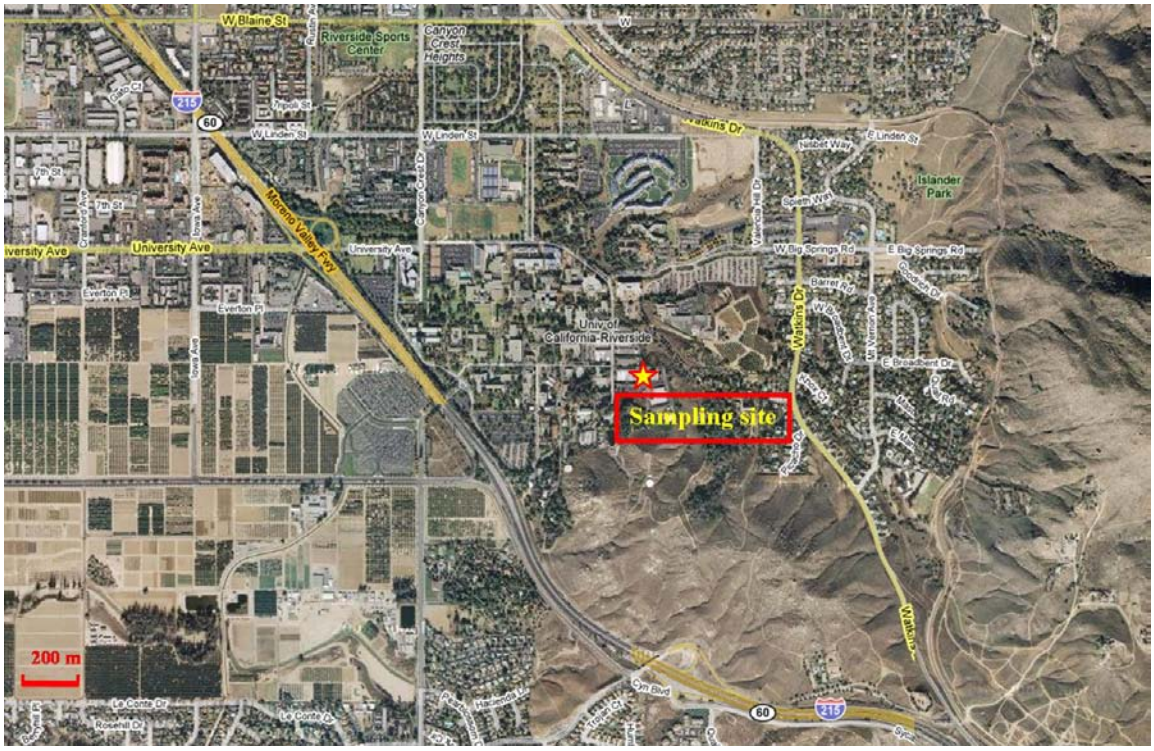

Figure 25: Map of SOAR sampling site on UCR campus.

measurements were also available. Both the ATOFMS and APS sampled off the same cylindrical stainless steel manifold which connected to the ambient atmosphere on one side with a single port and to several instruments on the other side through multiple ports. To prevent alteration of ambient aerosol composition, the sampling lines outside the mobile laboratory were covered with reflective insulation wrap to minimize the loss of semivolatile species during the daytime; the sampling lines inside the mobile laboratory were covered with insulated foam, placed inside of a large diameter plastic tubing and surrounded by constant flow of ambient air to prevent condensation of semivolatile species and water due to the temperature difference between ambient and mobile laboratory air.

The California Air Resources Board ambient air quality monitoring site at Rubidoux, CA is located ~10 km northwest of SOAR sampling site (149). Due to the absence of beta attenuation monitor (BAM) data at SOAR sampling site, ambient $PM_{2.5}$ mass concentrations are represented by Rubidoux BAM measurements, which are good estimates of the sampling site $PM_{2.5}$ levels during most of the study periods. Wind data, ambient temperature and relative humidity (RH), taken at the SOAR sampling site, were provided by the Goldstein group at University of California, Berkeley.

c. ATOFMS Data Analysis

The chemical composition and D_a of 1,076,812 and 1,061,506 ambient particles were collected using ATOFMS during SOAR-I and SOAR-II, respectively. The detailed

design and operating principles of ATOFMS are discussed in detail by Gard and co-workers (127). The desorption/ionization laser power used in the SOAR studies was 1.5 mJ, which has been shown to be able to fully ionize particles smaller than 1.0 μm (85). A custom software package was used to calibrate the mass spectra, and ion peaks were extracted into a peak list which were imported into Matlab using a single particle mass spectrometry data analysis tool, YAADA, for further analysis (160). The area and relative area of marker peaks in ATOFMS mass spectra can be related to the amount of specific species on each particle (85,161). To obtain major particle types over the study, an adaptive resonance theory-based clustering method (ART-2a) was used to classify ATOFMS measurements (35). By comparing the existence and intensity of ion peaks in single particle mass spectra, ART-2a classifies particles into separate clusters based on their mass spectral fingerprints. The "quintessential" mass spectra which represent the overall mass spectral characteristics of each cluster are referred to as its weight matrix. Submicron ($0.2\ \mu m \leq D_a < 1.0\ \mu m$) and supermicron ($1.0\ \mu m \leq D_a \leq 2.5\ \mu m$) particles during SOAR-I and SOAR-II were classified with ART-2a separately. A vigilance factor of 0.80 was used in this work, and particles in the most populated 50 (top 50) clusters account for ~90% of total ART-2a classified particles in both size ranges for SOAR-I and SOAR-II. Therefore, the top 50 clusters are representative of the overall aerosol composition and are the focus of this paper. The purpose of this paper is to present general pictures of major aerosol compositions over the course of the study during each season; thus information on unique species (such as metals) and distinct events will be the focus of future papers.

iii. Results and Discussion

General meteorological conditions exhibited diurnal variations for both seasons and are summarized in **Figure 26**. In summer, westerly winds dominated during the daytime between 6:00 and 18:00 reaching their maximum speeds at approximately 14:00. At night, the wind direction came from the east, associated with a decrease in wind speed. Temperature and O_3 concentrations showed similar diurnal trends as wind speed, while RH showed the opposite trend. Maximum temperature and O_3 concentrations and minimum RH were observed at approximately 14:00; minimum temperature and O_3 concentration and maximum RH occurred around 5:00. Overall, ambient meteorological conditions exhibited strong diurnal pattern without substantial day-to-day variation during SOAR-I.

Similar diurnal trends of wind speed, temperature, RH, and O_3 concentrations were still present during SOAR-II but the trend was weaker. Distinct differences were observed during certain periods including daytime wind directions. Easterly wind was observed at night throughout most sampling duration, which switched to westerly winds between 9:00 and 16:00 from November 2 to November 14. October 31 to November 1 and November 15 to November 21 were Santa Ana periods, during which warm, dry, and gusty offshore winds blows from the east-northeast to Southern California. Maximum wind speeds in SOAR-II (~1.6 m/s) were generally lower than those in SOAR-I (~2.5 m/s) except during the Santa Ana periods when wind speed can reach above 2.5 m/s. Moreover, wind speed spiked frequently in early mornings during SOAR-II besides the

daytime peak. Compared to SOAR-I, SOAR-II O_3 concentration displayed a similar diurnal variation with more irregularity during Santa Ana periods. However, the highest

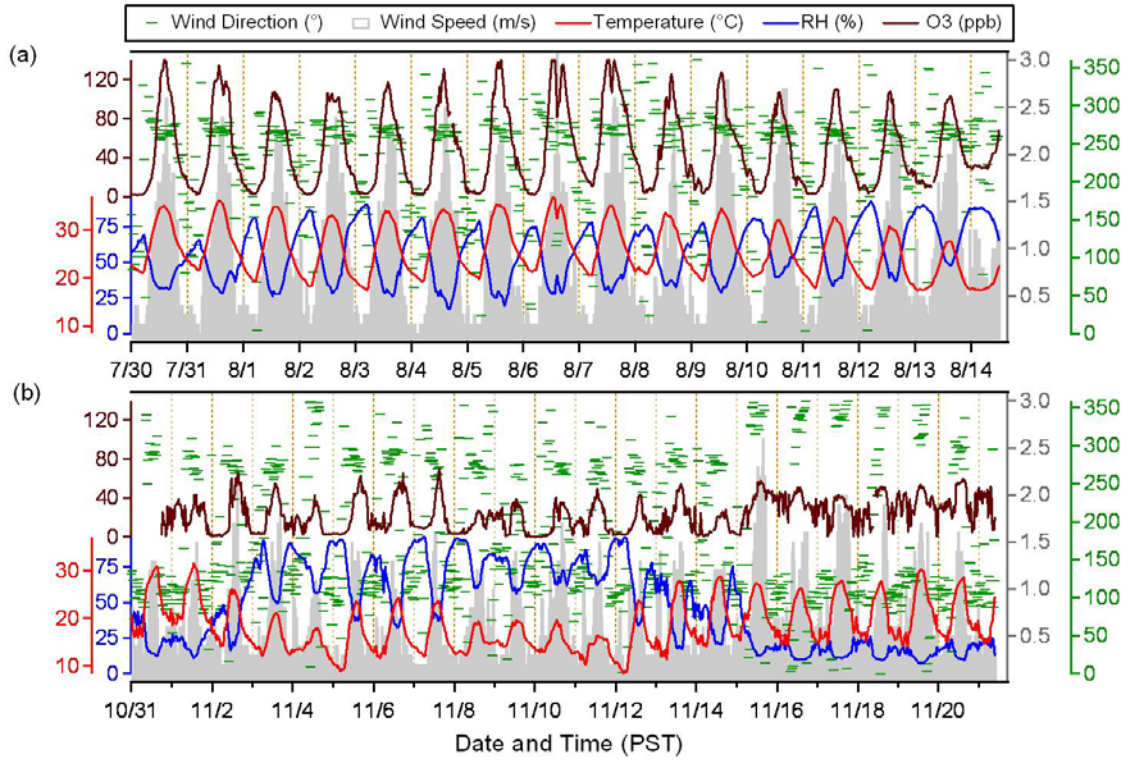

Figure 26: Temporal variations of ambient wind speed, wind direction, temperature, relative humidity, and ozone concentration during SOAR-I (a) and SOAR-II (b).

O_3 concentration throughout SOAR-II was only 70 ppb, whereas in SOAR-I, the daily O_3 concentration maximum frequently exceeded 100 ppb. SOAR-II will be segregated into more detailed episodes in the forthcoming sections.

a. $PM_{2.5}$ Concentrations

BAM mass concentrations and APS size-resolved number concentrations for ambient $PM_{2.5}$ are compared in **Figure 27** for both SOAR-I and SOAR-II. The contour plots represent hourly temporal and size-resolved APS number concentrations in log scale with red being the highest concentrations and purple being the lowest. Hourly BAM measurements (brown line) are superimposed on APS measurements for more clear comparison. In SOAR-I, $PM_{2.5}$ mass concentrations displayed diurnal variations peaking mostly around noon with 79 $\mu g/m^3$ being the highest concentration observed. This daytime peak was likely due to a combination of transport of LA morning traffic pollution and secondary aerosol formation from photochemical reactions, which was dissipated by the increase in wind speed in early afternoon hours (from ~1.5 m/s to 2.5 m/s). No consistent diurnal trend was observed in SOAR-II ambient $PM_{2.5}$ concentrations, but there were episodes of extremely low mass concentrations during Santa Ana periods, as well as a gradual buildup between November 2 and November 7 with the highest concentration of 106 $\mu g/m^3$ in the Fall.

APS number concentration measurements showed results consistent with BAM measurements. The highest number concentrations during SOAR-I typically occurred around noon in the size range of 0.5 – 1.0 μm, during which the BAM also displayed daily peaks. The particles between 0.5 – 1.0 μm account for majority of particle mass and have a larger size distribution due to aging compared to freshly emitted particles.

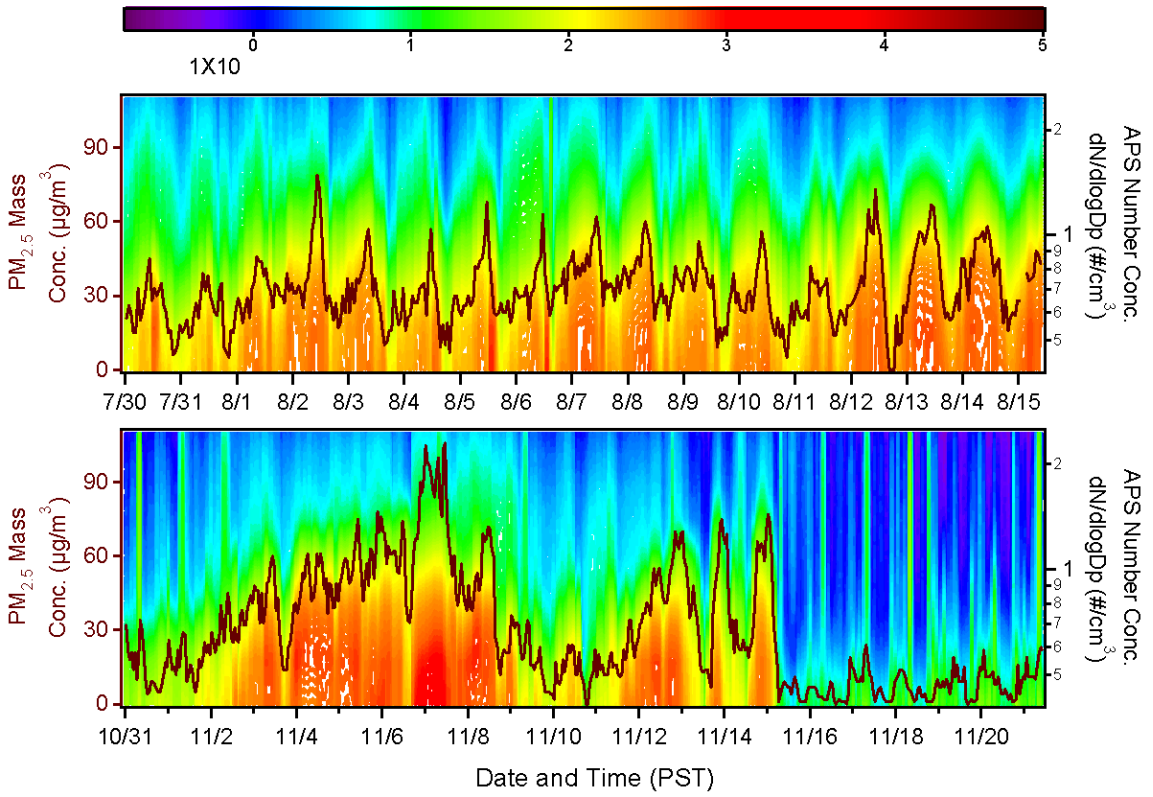

Figure 27: Hourly temporal variations of BAM $PM_{2.5}$ mass concentration and size-resolved hourly APS $PM_{2.5}$ particle number concentration during SOAR-I (top) and SOAR-II (bottom). Contour plots represent APS number concentration in log scale, and the red lines correspond to BAM data.

Late afternoons were generally characterized by the lowest particle number concentrations, which also agreed well with the trends shown by the BAM. SOAR-II episodes were also easily discerned with APS measurements. Similar to the agreement in SOAR-I, APS and BAM measurements displayed similar patterns in SOAR-II. Santa Ana periods featured extremely low number concentrations even in the smallest size ranges; a gradual buildup period between November 2 and November 7 was characterized by increased APS concentrations, with a maximum of >500 particles/cm^3 observed in the early morning of November 7. ATOFMS raw particle counts typically tracked well in both seasons with APS measurements having an R^2 of 0.59 in SOAR-I and 0.84 in SOAR-II.

b. Chemical Composition of ART-2a Clusters

The ART-2a weight matrices of major Riverside particle types have been presented previously by Pastor et al. (154). Most particle types in Pastor's work were observed in the current studies although a few clusters were categorized differently based on more experience with ATOFMS measurements. Similar particle classes dominated both SOAR-I and SOAR-II; however, their relative fractions were different. The association of clusters with secondary species provides important information on aerosol aging. As observed previously in Riverside, the most common secondary marker peaks in this study are m/z 18 (NH_4^+), 30 (NO^+), 86 ($C_5H_{12}N^+$), -46 (NO_2^-), -62 (NO_3^-), -80 (SO_3^-), -97 ($HSO_4^-/H_2PO_4^-$), and -125 ($HNO_3NO_3^-$). The peak at m/z 43 ($CH_3CO^+/CHNO^+$) is also a secondary marker photo-oxidation reaction. **Figure 29** showed SOAR-I temporal variation of O_3 concentrations and the hourly average peak area of m/z 43. They track each other very closely indicating that m/z 43

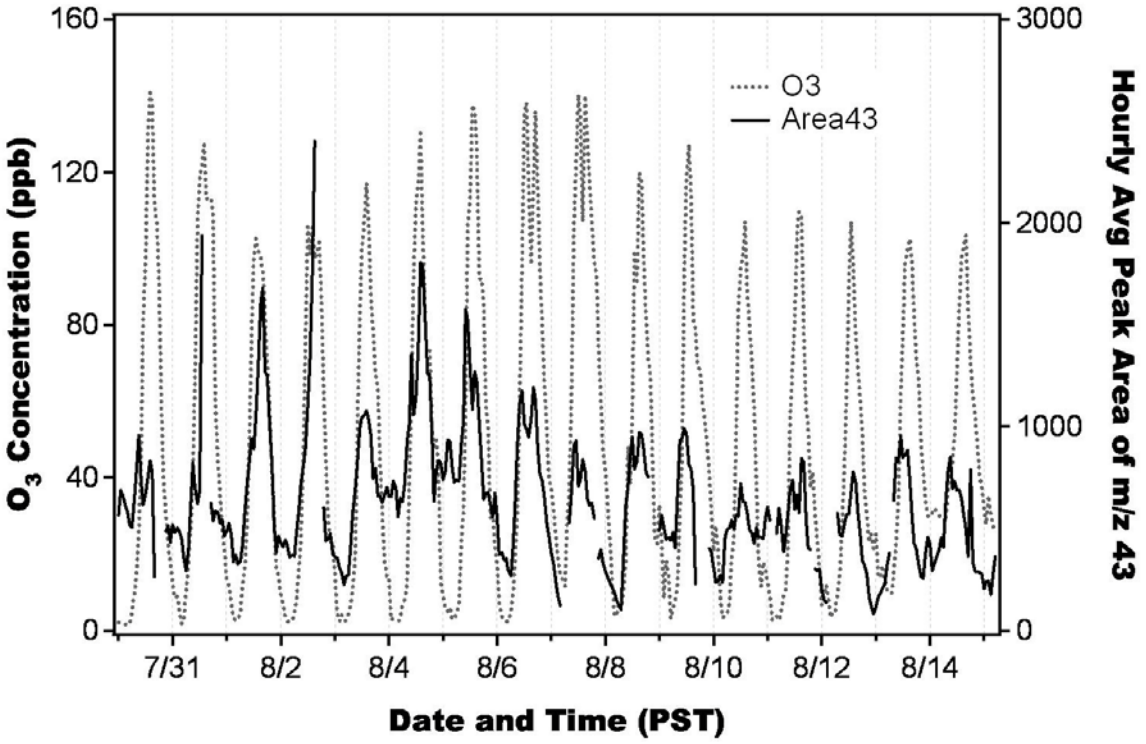

Figure 28: Hourly temporal variations of O_3 concentration and hourly average peak area of m/z 43.

(CH_3CO^+/$CHNO^+$) is a secondary marker indicative of photo-oxidation reaction. No similar correlation was observed during SOAR-II, possibly due to the decrease in O_3 concentrations. Overall, secondary organic aerosol concentrations are lower in the Fall (48,54).

Representative ART-2a weight matrices of the SOAR major particle types are included in **Figure 29**. Aged OC1 represent typical OC particles showing the most intense fragment peaks at m/z 27 ($C_2H_3^+$/CHN^+), 37 (C_3H^+), and 43; their mass spectra also contain low intensity peaks representing secondary species including 18, 30, 86, and 118 ($(C_2H_5)_3NOH^+$). No negative ions were detected for this particle type. Aged OC-SO_4 have similar positive mass spectral features as aged OC1; additionally, they have intense negative spectra showing associations with nitrate (m/z -46, -62 and -125) and sulfate (m/z -80 and -97). The positive spectra of ECOC contain both EC and OC signatures. These particles contain similar OC mass spectral patterns as aged OC1 and have no negative spectra, but the most intense positive peaks are from characteristic EC fragments at m/z 12 (C^+) and 36 (C_3^+) along with other low intensity EC peaks. ECOC-SO_4 particles have similar positive spectra compared to ECOC and similar negative spectra to aged OC-SO_4; these particles contain a mixture of OC, EC, nitrate, and sulfate. Vanadium-rich particles contain mostly OC in the positive spectra, with the dominant peaks being m/z 51 (V^+) and 67 (VO^+). Aged sea salt and biomass are both associated with nitrate and sulfate as shown in their negative spectra. The most intense positive peak of aged sea salt particles is the peak at m/z 23 (Na^+), followed by lower intensity m/z 81 (Na_2Cl^+), 108 ($Na_2NO_3^+$), 39 (K^+) and carbonaceous peaks. Hughes and co-

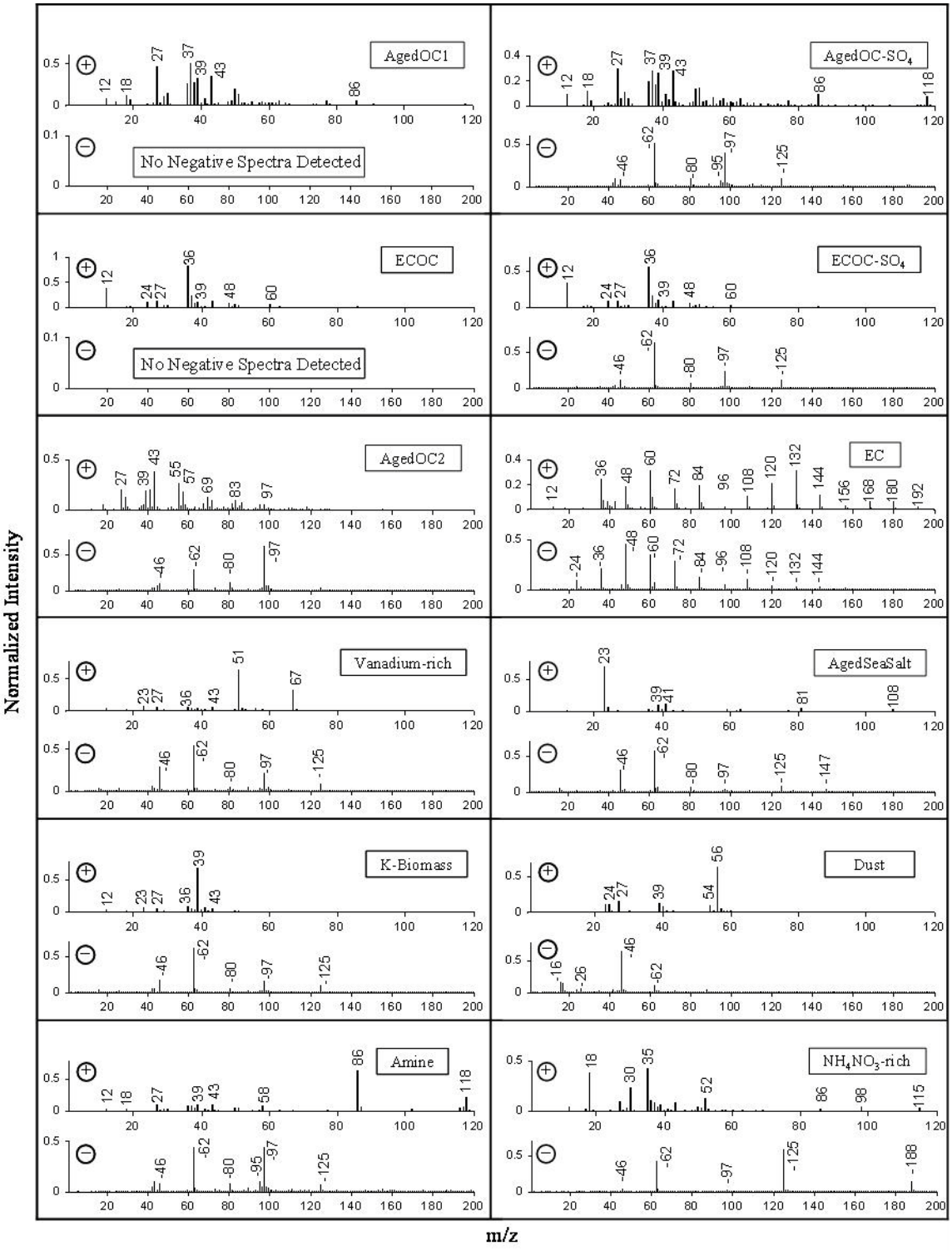

Figure 29: ART-2a weight matrices of representative particle types during SOAR-I and SOAR-II.

workers showed that sea salt is the only significant sodium source in Riverside (158). The most intense positive peak in biomass particles is m/z 39 (K^+) accompanied by low intensity OC peaks; many studies have shown that potassium is the marker for biomass emissions (162-164). Dust particles are mostly distributed in supermicron range and contain one or more inorganic species including sodium, magnesium, aluminum, silicon, potassium, calcium, iron, and manganese; the weight matrix of iron-rich particles is presented here as an example. The positive weight matrices of all the above particle types are consistent with the major ones presented previously in Pastor et al. (154). Having only single positive spectra limited the ability of Pastor et al. in differentiating between aged and fresh particle types (i.e. aged OC1 and aged OC-SO_4 and ECOC and ECOC-SO_4). These types are shown to have very different temporal variations in the following sections.

Four additional Riverside particle types were identified in the SOAR studies that were not shown in Pastor et al. EC is an elemental carbon dominant type showing very distinct continuous C_n^+/C_n^- patterns (where n is an integer) in both polarities extending beyond m/z 150. Amine particles are organic carbon particles with m/z 86 and 118 being the most intense positive peaks (39). NH_4NO_3–rich OC-containing particles are characterized by intense ammonium and nitrate cluster peaks in the positive spectra at m/z 18, 30, 35 ($(NH_3)_2H^+$), 52 ($(NH_3)_3H^+$), 98 ($(NH_3)_3NO_2H^+$), and 115 ($(NH_3)_4NO_2H^+$); their negative spectra are dominated by nitrate peaks. This type is quite different from the ammonium nitrate particles in Pastor et al., which mainly contain m/z 18 and 30 (154). Aged OC2 is a low abundance OC cluster (<2% on average). The positive spectra of this type show distinct envelope patterns peaking around m/z 27 and 29; 39, 41 and 43; 55 and 57; 69 and 71; 81 and 83; 95 and 97. Compared to particle types in Pastor et al., the most likely reasons for observing the above four particle types in the SOAR studies are classifying submicron and supermicron particles separately and using a higher vigilance factor, although we cannot exclude a change in the ambient air quality between 1997 and 2006. All particles during the SOAR studies show some degree of aging based on the associations between the major particle types and secondary ammonium, amines, nitrate, and sulfate.

c. SOAR-I Diurnal Variation

In SOAR-I, the fractions of the major particle types showed distinct diurnal trends throughout the sampling period. Submicron aerosols were dominated by carbonaceous particles; while supermicron aerosols were alternately governed by either carbonaceous particles or dust and aged sea salt particles depending upon the time of day. **Figure 30** a-d presents the hourly temporal variations of the number fractions of major particle types for the top 50 clusters, with BAM measurements superimposed on each plot in red trace. The following discussions of temporal variations refer exclusively to the ATOFMS particle type number fractions unless otherwise specified. Also included in **Figure 30** are the size distributions of total $PM_{2.5}$ in each season. **Figure 31** shows the size-resolved number fractions of each of SOAR-I top 50 ART-2a clusters at various time of day: 3:00, 9:00, 15:00 and 21:00. Clusters with similar chemical compositions are placed next to each other with the same theme color but various patterns and the data for each hour were obtained by taking the average of the same hour data over all sampling days. The size

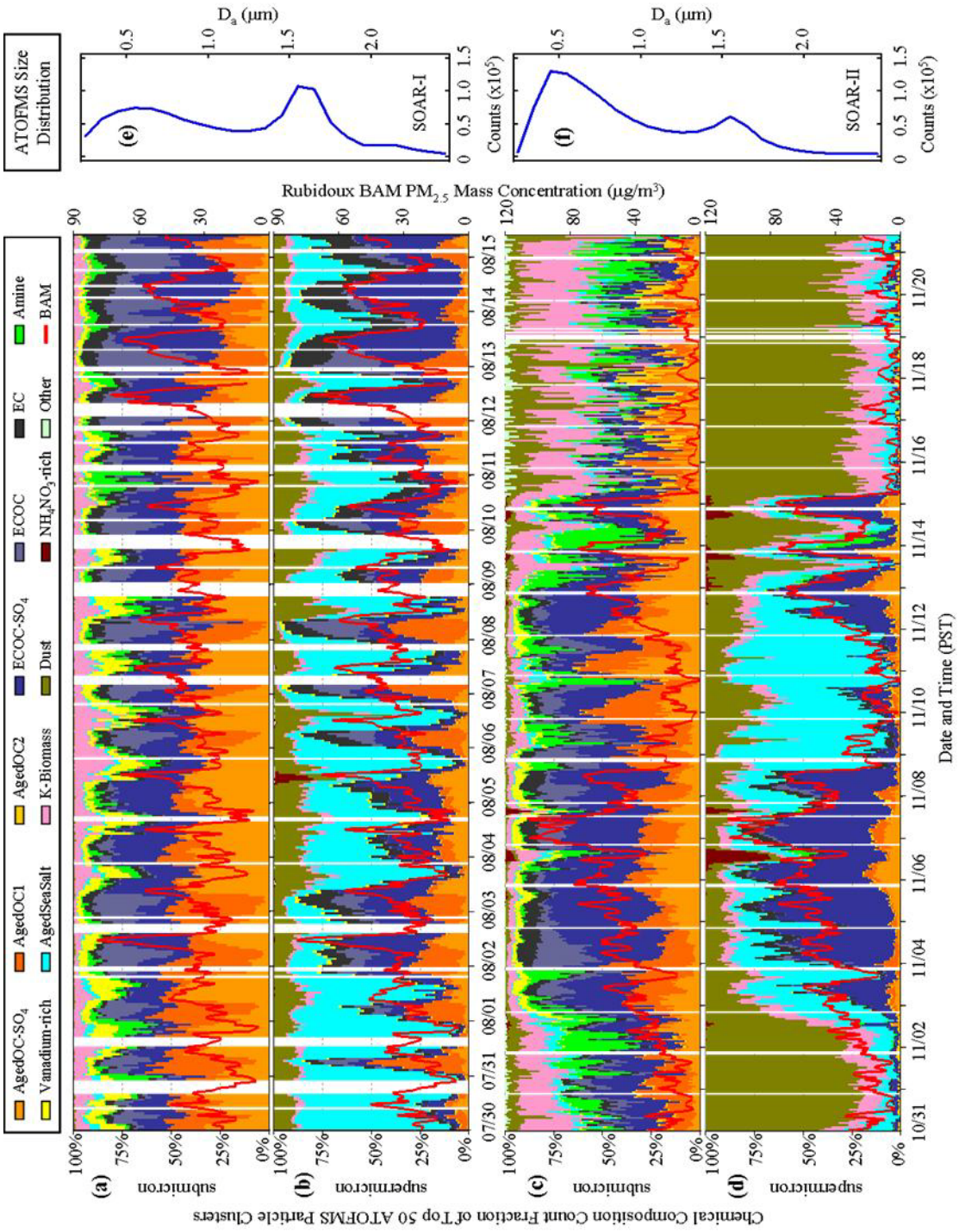

Figure 30: Temporal variations of the number fractions of major particle types for the top 50 clusters superimposed with PM2.5 mass concentrations (red line) and size distributions of total ATOFMS particle counts.

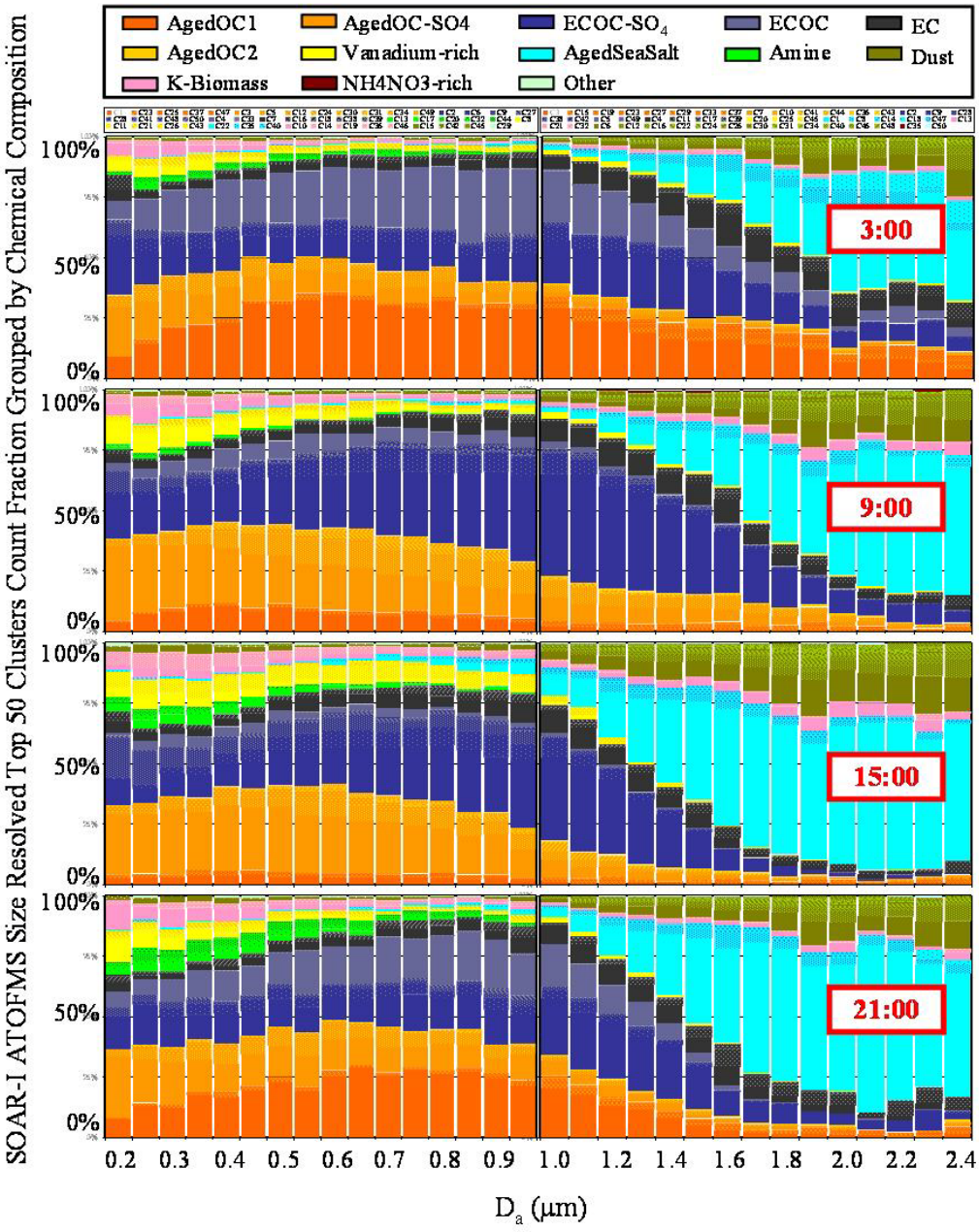

Figure 31: Hourly size-resolved number fractions of SOAR-I top 50 clusters from ART-2a results averaged for 3:00, 9:00, 15:00 and 21:00 over all sampling days. Size resolution is 0.05 μm for the submicron range and 0.10 μm for the supermicron range.

resolution is 0.05 μm for submicron and 0.1 μm for supermicron particles with the starting size indicated on the bottom axis.

SOAR-I aged OC1 and ECOC peaked in early morning around 5:00 as shown in **Figure 30 a-b**. These two types of particles only had positive spectra. They were likely the fairly aged aerosols experienced daytime photochemical reaction and nighttime aqueous phase processing, but high RH values in the early morning suppressed the

negative ions on these particles, causing them to peak at 5:00. EC showed a similar temporal trend and also peaked around 5:00. Based on the low intensity of secondary marker peaks, these particles were freshly emitted and were most likely from local vehicle sources. **Figure 31** presents complimentary information showing the highest aged OC1 and ECOC fractions appearing close to 3:00 in both submicron and supermicron ranges and lowest fractions were observed near 9:00 and 15:00, mainly distributed in the submicron range. EC, however mostly fell in the supermicron range, which is a little un-expected since freshly emitted particles are usually small in diameter (< 0.2 μm). There might be contributions from other local source that generate larger EC particles. The low wind speeds at night coupled with low inversion layers assisted the buildup of particles and led to the observed high carbonaceous fractions. Aged OC-SO_4 and ECOC-SO_4 mostly peaked subsequently later in the morning around 9:00 and showed a second peak around 14:00. The morning peaks likely correspond to transformed organic aerosols from early morning vehicle emissions and the time of the peaks was affected by local aerosol transformation rates. The afternoon peaks are due to the combination of local secondary aerosols formed through photochemical reactions and the transport of LA pollutants, which were originally emitted from LA early morning rush hour vehicles and were transported to Riverside by summer daytime westerly winds after about 8-10 hours as shown by the air mass trajectories. This afternoon peak was also observed in other studies, and the transport time have been estimated to range from a few hours to more than one day (151,165). Thus the variation in the afternoon peak hours was partly due to aerosol transport time. Aged OC-SO_4 were mostly submicron particles as shown in **Figure 31**. A substantial fraction of ECOC-SO_4 particles were in supermicron ranges, which possibly transformed from supermicron EC particles. Overall, carbonaceous particles mixed with nitrate, sulfate and ammonium dominated the submicron range throughout the day (75% - 90%), and were the major supermicron components in the morning periods.

Biomass, vanadium-rich, dust and aged sea salt particle types all peaked in the afternoon and were transported from the LA area by the daytime prevailing westerly wind. Biomass and vanadium-rich were mostly submicron particles; whereas dust and aged sea salt particles mostly fell in the supermicron range and when combined often comprised 90% of supermicron particle counts at their maxima. Dust particles also displayed a minor peak in the morning, which is likely from local sources. **Figure 31** also shows that aged sea salt and dust governed the supermicron range especially around 15:00 in the largest size bins. Vanadium has been observed in particle phase in many studies and are one of the major metal components of ship emissions (166-168). Although a minor fraction can be emitted from vehicle exhaust (36), the vanadium-rich particles during the SOAR studies were most likely emitted from ships in LA and Long Beach Harbors and were transported inland to Riverside. Vanadium measurements by Singh and co-workers in Riverside (169) show consistent results where vanadium concentrations peak from late afternoon to early evening; however, the major source of vanadium was proposed to be vehicle emissions instead of ship engine exhaust in their paper (169). As shown in **Figure 31**, SOAR-I vanadium-rich particles peaked around 15:00. The highest fractions of vanadium particles occurred in the low submicron size range, indicating that these particles were generated from combustion sources instead of crustal material, and grew to fine range during transport.

Amine particles were associated with both nitrate and sulfate. They were only observed in the submicron range and peaked between 17:00 and midnight as shown in **Figure 30** and **Figure 31**. Similar diurnal variations of ambient amine particles have been observed in previous studies in Riverside and Atlanta (39). Amine particles are small in diameter and are semivolatile because they are formed through photo-oxidation of gas-phase low molecular weight amine. (39). Therefore, most amine particles were detected at night when they participated into particle phase at low ambient temperature and high RH (39). The highest amine fractions occurred in the smallest size bins.

NH_4NO_3-rich particles represented highly aged aerosols containing a great amount of ammonium and nitrate as demonstrated by their weight matrix. These particles mostly fall into the supermicron range due to particle growth during aging as shown in **Figure 30 a-b**. High NH_4NO_3-rich particle fractions occurred around noon on August 5, as well as less distinguishable spikes from August 2 to August 9 around the same time in SOAR-I. High concentrations of nitrate particle precursors were generated from LA area morning vehicle emissions and formed nitrate as the particles were transported inland. Large amounts of NH_4NO_3 were produced when the high concentration nitrate particles crossed Chino dairy farm area upwind and were continuously transported east causing sharp spikes (3-5 hrs) in Riverside NH_4NO_3 concentrations. Similar NH_4NO_3 production mechanisms in Riverside have been proposed previously by Kleeman and Cass and by Singh and co-workers (169,170). Hughes and co-workers observed a higher mass fraction of NH_4NO_3 in particles in 1.0-1.8 μm compared to 0.56-1.0 μm during filter analysis, which is consistent with the higher NH_4NO_3-rich particle fractions in the supermicron range by ATOFMS (150,153). Single particle analysis by Pastor et al. showed a temporal anti-correlation between sea salt and NH_4NO_3 particles (154). This anti-correlation is not observed in the SOAR studies; in fact the relative fractions of aged sea salt and NH_4NO_3-rich particles sometimes peak around the same time.

Overall, the SOAR-I particles are fairly aged, and most particle types displayed distinct diurnal variations. Total carbonaceous fractions were high from late night to late morning, whereas amine, vanadium-rich, biomass, and aged sea salt fractions peaked in late afternoons. The daytime was greatly influenced by LA pollutants due to the prevailing westerly wind; nighttime was affected by low speed easterly wind, thus local emissions dominate aerosol composition. In most cases, BAM measurements showed maxima when carbonaceous particle fractions were the highest, indicating that carbonaceous particles which associated with nitrate, sulfate and ammonium were the major $PM_{2.5}$ components by mass.

d. SOAR-II Episodic Variations

While SOAR-I and SOAR-II had similar major particle types, episodic temporal variations were observed in SOAR-II particles fractions as shown in **Figure 30 c-d**. Although no consistent diurnal trends exist with the exception of the NH_4NO_3-rich, SOAR-II sampling period can be characterized into unique episodes based on ambient $PM_{2.5}$ mass concentration levels. Specifically, the episodes are: SantaAna1, October 31 0:00 – November 1 19:00; Buildup1, November 1 19:00 – November 6 15:00; HighMass, November 6 15:00 – November 7 18:00; Buildup2, November 7 18:00 – November 8

22:00; Scavenging, November 8 22:00 – November 11, 13:00; Buildup3, November 11 13:00 – November 15 5:00; and SantaAna2, November 15 5:00 – November 21 10:00.

Figure 32 presents the hourly-averaged size distributions of the top 50 clusters number fractions during each episode. Similar to **Figure 31**, clusters with the same composition are positioned next to each other and represented with the same color but different patterns. Submicron and supermicron size distributions are shown with size resolutions of 0.05 μm and 0.10 μm, respectively. The $PM_{2.5}$ mass concentrations within each respective episode are highlighted in green in **Figure 32**. Also included are seven representative HYSPLIT 48-hour back trajectories ending at Riverside with 4-hour time resolution (171). The HYSPLIT trajectories provided the origin of the air mass during each episode; the total traveling distance correlates with the speed of air mass movement. The end times of each trajectory correspond to one day in each episode at 6:00. All of the HYSPLIT plots in **Figure 32** have the same latitude-longitude scale except for SantaAna2, during which the air mass traveled very far during the past 48 hours; therefore, a much larger geographical region is needed to display the complete

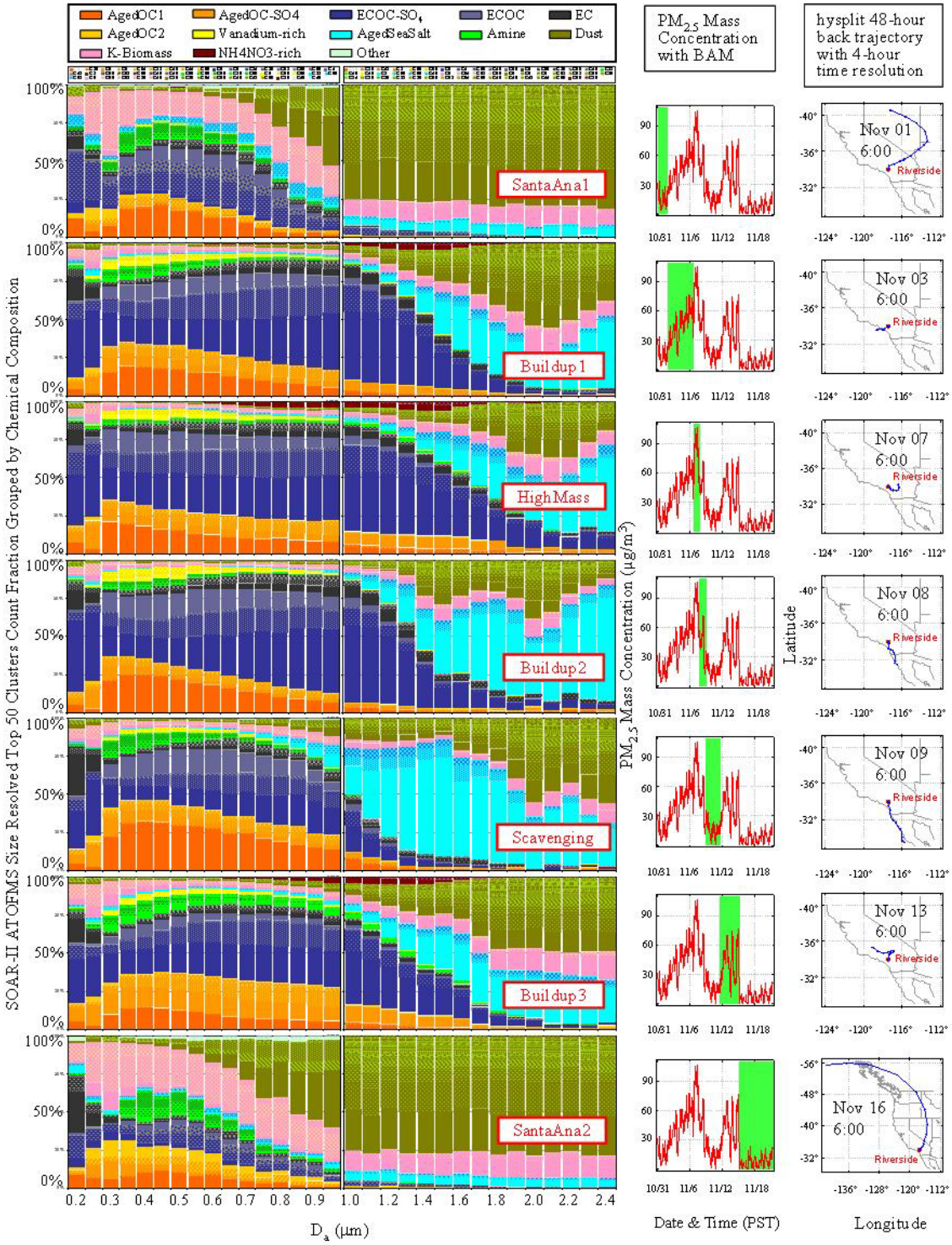

Figure 32: Size-resolved number fractions of SOAR-II top 50 clusters from ART-2a results averaged over each episode along with corresponding PM2.5 levels and representative 48-hour HYSPLIT back trajectories.

trajectory. All of the back trajectories illustrated the common conditions for each episode; while particular hours within the episodes could have different trajectories, they are not representative of the general conditions.

In addition to the low ambient particle mass and number concentrations, low RH and high temperature are the distinct characteristics of both Santa Ana periods. HYSPLIT back trajectories in **Figure 32** show that SantaAna1 air mass reaching Riverside at 6:00 on November 1 started from Nevada 48 hours before and consecutively traveled east through Utah, Arizona, then west to Nevada, California, and finally reached the sampling site. The air mass traveled a much greater distance compared to the non-Santa Ana periods and carried a large amount of dust particles to Riverside, while taking away many of the carbonaceous particles to the west. Even faster air mass transport was observed during the SantaAna2 period. The air mass ending at 6:00 on November 16 traveled east from the Gulf of Alaska through Canada, then south to the US during the past 48 hours. The stronger weather condition in SantaAna2 led to lower APS counts, lower $PM_{2.5}$ mass concentrations, and lower carbonaceous fractions comparing to SantaAna1. Consistent with the trajectory plots, ATOFMS measurements observed great fractions of dust particles during Santa Ana periods due to the desert influence. **Figure 30** and **Figure 32** show that carbonaceous (~50% of total counts), biomass, amine, and dust types were the major components of submicron particles; whereas supermicron particles were composed of ~75% dust, ~15% biomass and ~5% aged sea salt with very low (<5%) carbonaceous fractions in these episodes. The particle type fractions in **Figure 30c** do not appear as smooth during SantaAna2 as in other days, due to the low particle counts detected in this period. Substantial fractions of amine and biomass particles were observed; however, the increases in their relative fractions were most likely caused by much lower overall particle counts, and the actual counts for the two types were in fact lower than those during other episodes. These types are more likely emitted from local sources due to the absence of an LA influence. Vanadium-rich particle fractions were extremely low since they are mostly generated from ship emissions from the west, and the Santa Ana air masses originated from the eastern desert.

High RH and low temperature aided aerosol accumulation during Buildup1. The representative HYSPLIT trajectories show that the air mass was fairly stagnant during this episode resulting in a gradual increase of $PM_{2.5}$ mass concentrations with daily maxima occurring in the daytime. APS measurements showed consistent results with the BAM and also peaked during the day as shown in **Figure 27**. Carbonaceous particles not only dominated the submicron range, but also the supermicron range. Among the major particle types, aged OC1 spiked more at night due the effect of RH and ECOC-SO_4 peaked more during the day, which is consistent with SOAR-I patterns. The west-originating air mass and the accumulation aided in the formation and buildup of NH_4NO_3, therefore substantial fraction of NH_4NO_3-rich particles were observed in the supermicron range peaking around 1.5 μm.

HighMass was a 27-hour episode spanning overnight from November 6 15:00 to November 7 18:00 when the highest concentrations of the Fall study were observed. The stagnant meteorological conditions featuring 10-hours of low wind speeds led to the highest $PM_{2.5}$ particle number and mass concentrations (>500 particles/cm^3, 106 μg/m^3) on November 7 0:00 – 6:00. Once again, carbonaceous particles which were associated with nitrate, sulfate and ammonium accounted for more than 85% below 1.0 μm, and also

dominated the supermicron range. NH_4NO_3-rich particles were also observed in the HighMass period. Besides the large particles fraction in submicron range, NH_4NO_3-rich particles even spread into supermicron range due to the very stagnant condition. These particles only occurred during high ammonium nitrate episodes. Ambient mass concentrations started to decrease midday on November 7 as the wind speed rose.

The highest mass concentrations in Buildup2 occurred around noon on November 8. Air masses during this episode traveled north along the coast of Baja from Mexico to San Diego, eventually moved inland to Riverside. Thus, ATOFMS measurements show carbonaceous particles in the submicron mode, as well as an increased fraction of aged sea salt in the supermicron range due to a marine influence. No NH_4NO_3-rich particles were observed during this episode because the air mass did not pass over the Chino dairy area. The Scavenging episode featured very low particle number and mass concentrations due to precipitation events on November 9 and 10. Air mass back trajectories and major particle fractions are similar to those in Buildup2, however, aged sea salt dominate the supermicron range with low carbonaceous fractions. Finally, Buildup3 was a particle buildup period. Aerosol mass concentrations gradually increased on November 11 and 12 and displayed diurnal variations between November 13 and November 15 showing maxima at night. The air mass originated from the west and thus similar particle types were observed compared to Buildup1, with substantial NH_4NO_3-rich particles.

The only SOAR-II particle type that showed distinct diurnal variations was the NH_4NO_3-rich type. Four distinct NH_4NO_3-rich particle spikes appeared in both size ranges around November 6 12:00, November 7 15:00, November 13 18:00, and November 14 18:00, along with minor spikes shown in **Figure 30 c-d**. Most peaks occurred slightly later between 15:00-17:00 comparing to SOAR-I NH_4NO_3-rich type. Although SOAR-I NH_4NO_3-rich type peaked around 11:00 (PST), the actual local time corresponded to 12:00. The time delay between summer and fall NH_4NO_3-rich peaks is likely caused by the longer time required to form nitrate due to weaker solar radiation in the fall. The filter analysis by Hughes et al. showed that ammonium and nitrate fractions peak between 14:00 and 18:00 over October 31-November 1 in 1997, similar to the ATOFMS measurements in SOAR-II (150). Again, the NH_4NO_3 particles were formed as the nitrate particles crossed the upwind Chino area. Additionally, each NH_4NO_3-rich peak was followed by a high PM mass concentration spike; thus high ambient NH_4NO_3 levels could be one of the factors triggering high ambient mass concentrations. Similar behavior was observed by Turkiwicz et al. where NH_4NO_3 drove the $PM_{2.5}$ exceedances in San Joaquin Valley (172). Similar to SOAR-I, the temporal variations of the BAM measurements tracked carbonaceous particle number fractions, especially in the supermicron range, indicating that carbonaceous particles with nitrate, sulfate and ammonium are the major components in mass concentrations.

e. SOAR-I and SOAR-II Comparison

Although similar ATOFMS particle types were observed in both SOAR-I and SOAR-II, temporal variations and particle fractions of major types were different in summer and fall. In general, the submicron size range was dominated by carbonaceous particles and the major particle types in supermicron range were aged sea salt, dust and carbonaceous, except during the Santa Ana periods when dust dominated. The top OC

and EC types are very similar in both summer and fall, and no new major particle type was observed in either season.

Figure 30 e-f shows the raw particle size distributions measured by ATOFMS during SOAR-I and SOAR-II with a resolution of 0.10 μm. Despite the size-dependant transmission efficiency (173), the SOAR-I particle size distribution peaked around 1.6 μm with more supermicron particles detected than submicron particles; whereas the size distribution in SOAR-II peaked around 0.5 μm, dominated by submicron particles. The differences in size distributions are indicative of various degrees of aerosol aging. SOAR-I particles were highly transformed through photochemical reactions and other reaction pathways. Particles grew in size during aging, leading to high supermicron particle counts. SOAR-II particles were less aged thus their original sizes were not altered as much through processing. The decrease in solar radiation during the fall is one reason for the reduction in aerosol aging. It is also evident that higher fractions of aged OC (aged OC1+aged OC-SO_4) were observed in SOAR-I than SOAR-II, further indicating that SOAR-I aerosols were more aged than SOAR-II aerosols.

The ternary plots of SOAR-I and SOAR-II representative submicron aged OC-SO_4 particles (~300 particles evenly distributed over the study period) are included in **Figure 33**. These plots showed the relative amount of nitrate, sulfate and ammonium on every single particle. A particle mostly containing nitrate (m/z -62) would appear at the lower left vertex; a particle mostly containing sulfate (m/z -97) would appear at the lower right vertex; a particle mostly containing ammonium (m/z 18) would appear at the top vertex. SOAR-I aged OC-SO_4 particles evenly distributed between nitrate and sulfate

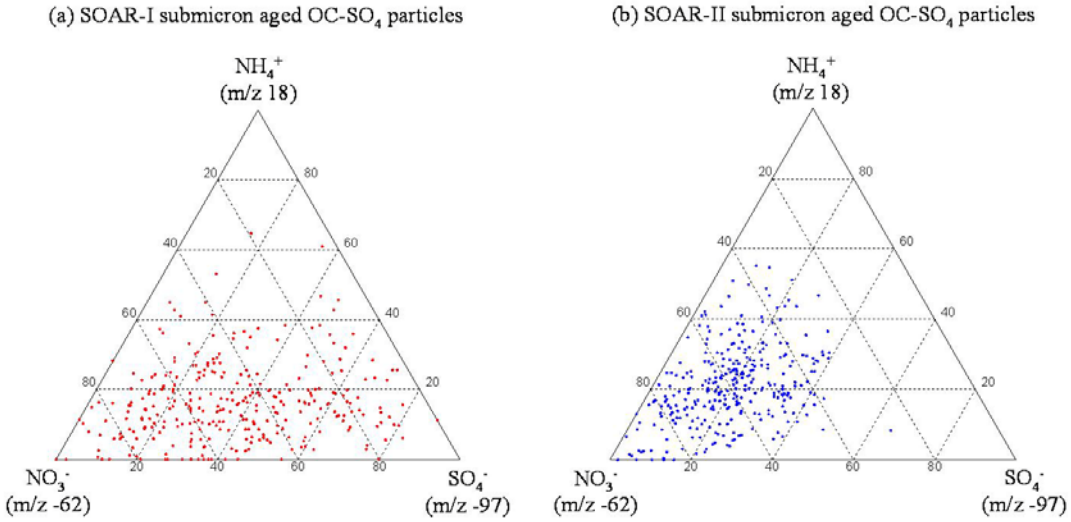

Figure 33: Ternary plots of SOAR-I and SOAR-II submicron aged OC1 particles. In each plot, a particle mostly containing nitrate would appear at the lower left vertex, a particle mostly containing sulfate would appear at the lower right vertex, a particle mostly containing ammonium would appear at the top vertex.

vertex, showing that the amount of nitrate and sulfate were comparable on these particles. In contrast, SOAR-II aged OC-SO_4 particles mostly distributed near lower left corner, illustrating that SOAR-II particles contained more nitrate than sulfate. Suring SOAR-I, ammonium and nitrate were baked off particle phase due to the high ambient temperature, thus there comparable amount of sulfate and nitrate in the particle phase; whereas the lower temperature in SOAR-II favors the condensation of ammonium and nitrate onto the particle phase, thus more nitrate was observed than sulfate, and ATOFMS detected the NH_4NO_3-rich particles during the Buildup and HighMass periods. Secondary processing of ambient aerosols will be addressed in detail in future papers.

The mass concentrations of major particle types during SOAR-I and SOAR-II are shown in **Figure 34**. The mass concentrations were obtained by scaling ATOFMS measurements with APS measurements, and the detail of scaling is discussed in Chapter 5. The sum of the major particle type mass concentrations has similar trend as the $PM_{2.5}$ mass concentrations for both SOAR-I and SOAR-II. While the major particle chemical compositions were similar in the summer and fall, these seasons were dominated by different aerosol formation mechanisms and showed different temporal trends in major particle type mass concentrations. The LA influence was observed in the current work, and carbonaceous particles associated with secondary species were found to be the major $PM_{2.5}$ component by mass in Riverside. The detailed analysis of SOAR-I and SOAR-II ATOFMS measurements in this paper provide further understanding on ambient aerosol composition, chemical associations on a single particle level, and provide important information on ambient aerosol aging process in the LA basin and similar areas with strong vehicular emission influence and intense sunlight.

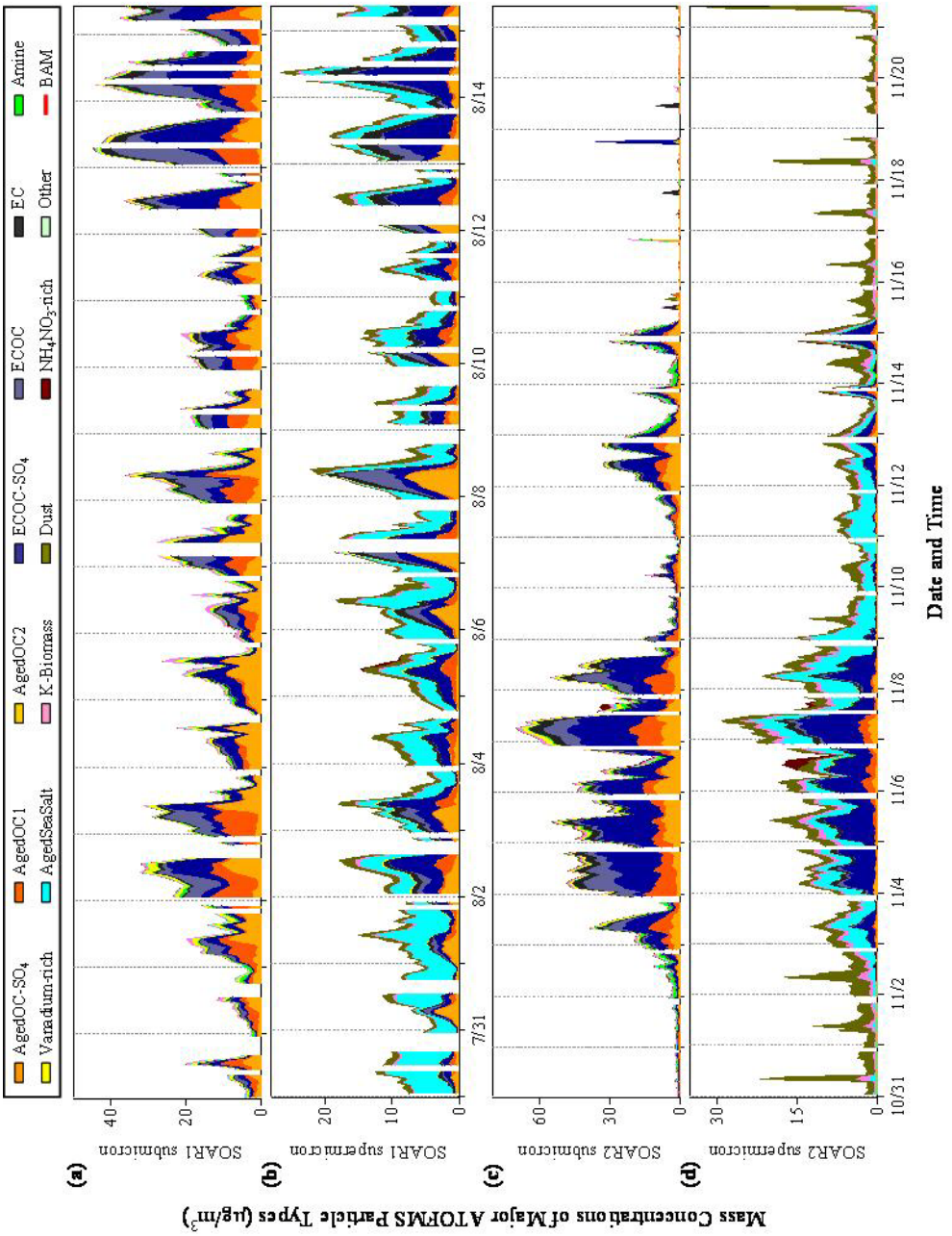

Figure 34: Temporal variation of the mass concentration of major ATOFMS particle types. Mass concentrations are obtained by scaling ATOFMS measurements with APS measurements.

iv. Acknowledgements

This research was supported by the California Air Resources Board (CARB) through Grant #04-336. The authors gratefully acknowledge the entire Prather group for their help throughout these studies, in particular, Ryan Sullivan, Kerri Denkenberger, and Dr. Hiroshi Furutani. We thank Professor Paul Ziemann and Professor Jose-Luis Jimenez for organizing this study and providing lab space to accommodate research instruments and Dr. Kenneth Docherty for coordination. We also thank Megan McKay and the

Goldstein research group at the University of California, Berkeley for providing meteorology data and CARB for providing BAM measurements. Finally, we acknowledge the NOAA Air Resources Laboratory (ARL) for providing the HYSPLIT transport and dispersion model used in this publication.